Journal of Medicinal Chemistry

pubs.acs.org/jmc

Article

One- and Two-Photon Uncaging of Carbon Monoxide (CO) with Real-Time Monitoring: On-Demand Carbazole-Based Dual CO-Releasing Platform to Test over Single and Combinatorial Approaches for the Efficient Regression of Orthotopic Murine Melanoma *In Vivo*

Yarra Venkatesh,[#] Venugopal Vangala,[#] Rakesh Mengji, Amrita Chaudhuri, Sayantan Bhattacharya, Prasanta Kumar Datta, Rajkumar Banerjee, Avijit Jana,[*] and N. D. Pradeep Singh[*]

Cite This: *J. Med. Chem.* 2022, 65, 1822−1834

Read Online

ACCESS | Metrics & More | Article Recommendations | Supporting Information

ABSTRACT: Herein, we report three new metal-free, photochemically active single, dual, and combinatorial CORMs (photoCORMs) based on a carbazole-fused 1,3-dioxol-2-one moiety which released one equivalent of CO, two equivalent of CO, and a combination of one equivalent of each CO and anticancer drug upon one- and two-photon excitation, respectively. The photoCORMs exhibited good cellular uptake and real-time monitoring ability of CO uncaging by a color change approach in cancerous B16F10 cells. Interestingly, the cytotoxicity assay on B16F10 cells indicated that the dual photoCORM has increased anticancer activity over the single and combinatorial photoCORMs upon irradiation. Our results also showed that CO could accelerate the effectiveness of the well-known anticancer drug (chlorambucil). Finally, the *in vivo* evaluation of the dual photoCORM on an established murine melanoma tumor (C57BL/6J mouse model) manifested a significant regression of tumor volume and led to significant improvement (>50%) in the overall survivability.

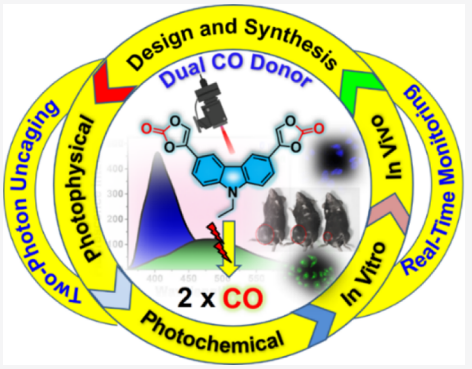

INTRODUCTION

Carbon monoxide (CO) is an important cell signaling molecule produced endogenously in mammals by enzymatic heme metabolism.[1] CO exhibits therapeutic potentials, including cytoprotective, antibacterial, and anti-inflammatory at low and safe doses.[2] Clinical trials have shown that the safe dose for inhaled CO is 250 ppm, 3 h/day.[3] Nowadays, several research groups are involved in exploring the anticancer activity of CO molecules by administering them in safe doses. A recent research study by the team at the Beth Israel Deaconess Medical Center (BIDMC) has shown for the first time that carbon monoxide plays a vital role in the treatment of cancer. Their studies based on cell culture and animal models suggest that controlled doses of CO within the prescribed safe limit prevent tumor growth and improve chemotherapeutic drugs' effectiveness to accelerate cancer cells' death while protecting non-cancerous tissues.[4] Following the above findings, several other research groups, have also reported the anticancer efficacy of the CO molecule.[5−7] However, to utilize the significant anticancer ability of CO for practical applications, two critical shortcomings need to be addressed (i) lack of precise control release of CO at a specific location for the given period and (ii) difficulty in portability. Hence, there is a real need to develop carbon monoxide releasing molecules (CORMs), which can provide a spatial and temporal control over the CO release and enable us to understand the anticancer properties of CO completely.

In this context, small molecules with controlled CO release have been developed based on different triggering mechanisms, which include enzyme,[8] magnetic heating,[9] and an interesting "click and release".[10] However, the main limitation of the above strategies was their inability to provide a spatio-temporal release of CO. To achieve a spatio-temporal release, researchers have introduced the photochemically active CORMs (photoCORM). To date, two types of photoCORMs are reported as CO donors (i) metal carbonyl complexes and (ii) small organic molecules. Compared to the possible disadvantage of metal carbonyls,[11,12] which often have a background CO release due to the ligand exchange, metal-free

Received: April 26, 2021
Published: January 12, 2022

https://doi.org/10.1021/acs.jmedchem.1c00750
J. Med. Chem. 2022, 65, 1822−1834

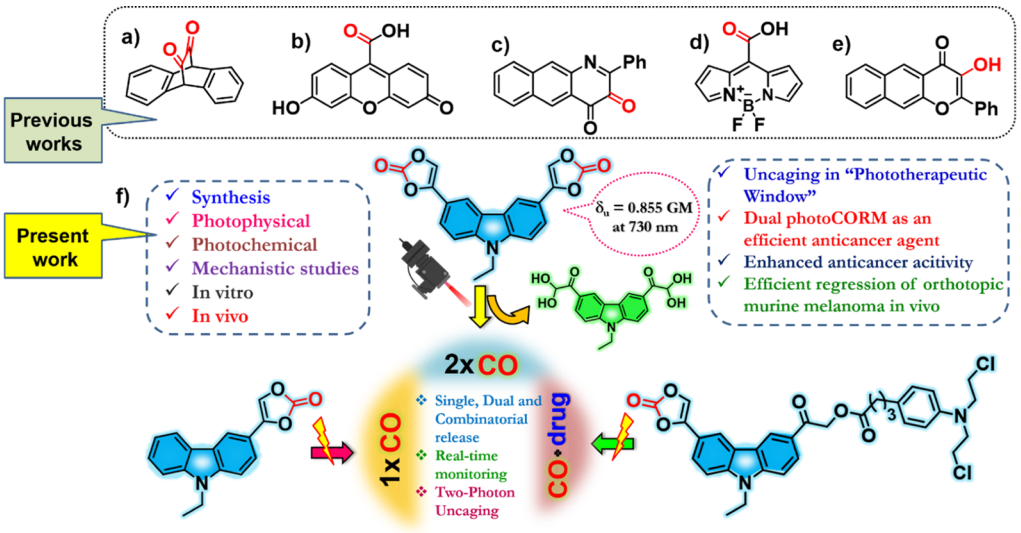

Figure 1. (a–e) Previous works: (a–c) Visible light-activated photoCORMs for one and two equiv of CO release, (d,e) NIR and two-photon activated photoCORMs for one equiv of CO release. (f) Present work: Designed one- and two-photon activated single, dual, and combinatorial photoCORMs with real-time monitoring for the release of one equiv of CO, two equiv CO and one equiv of both CO and Cbl, respectively.

Scheme 1. Synthesis of Single (3), Dual (5), and Combinatorial (8) photoCORMs

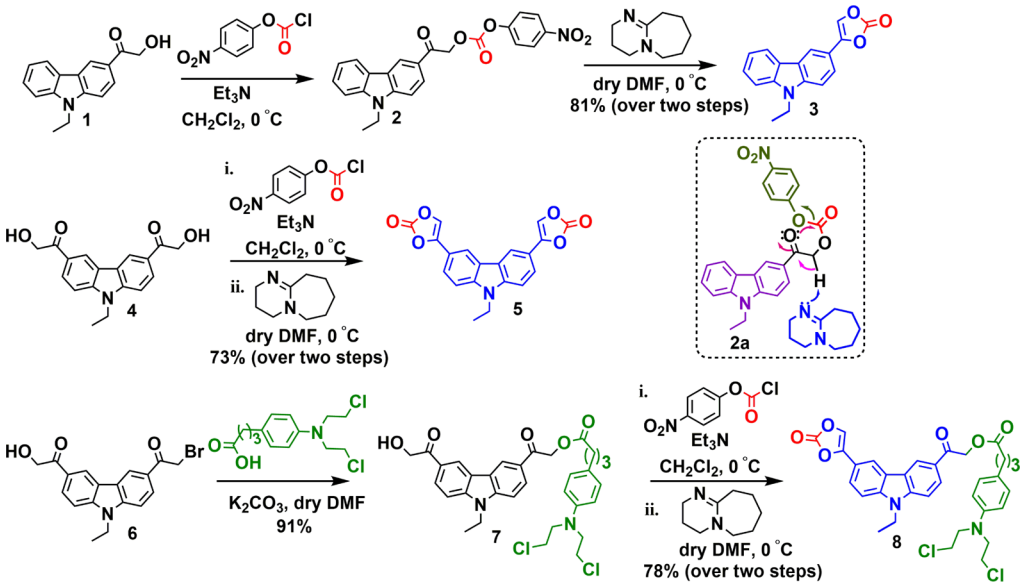

organic photoCORMs captured great attention for highly controlled CO release. To date, several UV[13−16], and visible light-activated photoCORMs such as cyclic aromatic α-diketone,[17] a fluorescein analog: 6-hydroxy-3-oxo-3*H*-xanthene-9-carboxylic acid,[18] flavonols,[19−21] and 3-hydroxybenzo-[g]quinolone frameworks[22] were developed (see Figure 1a–c). However, these photoCORMs limit their practical usage in biomedical applications because of the cytotoxicity and limited tissue penetration (typically not more than 1 mm) ability of UV light. Therefore, a new photoCORM, which could be effectively triggered by NIR light with minimal side effects in living tissue, is in great demand.

The release of bioactive molecules in the NIR region by two-photon excitation has gained considerable importance because it offers unique advantages such as (i) spatiotemporal resolution of uncaging, (ii) deeper penetration into biological tissue (up to 10 mm) with lower phototoxicity, and (iii) ability to restrict excitation to a tiny focal volume.[23−25] Literature studies clearly show that only two organic photoCORMs were recently developed, which can be activated in the "photo-therapeutic window (650–950 nm)". In 2016, Klán et al. reported meso-carboxy BODIPY (COR-BDP) derivatives as efficient photoCORMs for the release of CO in the visible-to-NIR (up to 730 nm) region (Figure 1d).[26] Later, Wang and Tang et al. in the year 2018 developed a two-photon activated flavanol conjugate for the CO release (Figure 1e).[27] Though the abovementioned photoCORMs efficiently uncages CO in the NIR region, still, they have some critical limitations such as (i) inability to provide information regarding the release of CO in real-time, which is crucial for a profound understanding of the biological benefits of CO, (ii) release of only one equiv of CO molecule at a given time, which limits the delivery of an effective amount to the target, and (iii) requirement of an external agent such as molecular oxygen to release CO.

https://doi.org/10.1021/acs.jmedchem.1c00750
J. Med. Chem. 2022, 65, 1822−1834

Keeping the above limitations of photoCORMs in mind, we intend to develop new metal-free photoCORMs based on a carbazole fused 1,3-dioxol-2-one platform to investigate two key features: (i) the effect of CO dosage on its anticancer efficacy and(ii) the role of CO in accelerating the therapeutic potential of the well-known anticancer drug. For this purpose, we synthesized three photoCORMs based on a carbazole platform, namely, single, dual, and combinatorial, for the release of one equivalent (equiv) of CO, two equiv of CO, and one equiv of both CO and the anticancer drug (chlorambucil) respectively. Our newly developed carbazole-based photoCORMs showed essential qualities such as (i) spatio-temporal uncaging in the "phototherapeutic window" at 730 nm using two-photon excitation, (ii) real-time monitoring of the CO release by fluorescent color change, and (iii) no need to use any external reagents to release CO, except light.

RESULTS AND DISCUSSION

Single, dual, and combinatorial photoCORMs (**3**, **5**, and **8**, respectively) were synthesized, as outlined in Scheme 1. Compounds **1**, **4**, and **6** were prepared according to the literature procedure.[28,29] Single photoCORM **3** was synthesized in two consecutive steps. In the first step, compound **1** was converted to the corresponding chloroformate (**2**) by treating with one equivalent of 4-nitrophenyl chloroformate (PNPCl). In the second step, the reaction between **2** and 1,8-diazabicyclo [5.4.0] undec-7-ene (DBU) produced 81% of single photoCORM **3**. The reaction mechanism for the second step involves the abstraction of α-hydrogen of the methylene ($-CH_2$) group by a strong base DBU, which leads to the enolization, followed by a five-membered ring formation with the removal of the leaving group, that is, *p*-nitrophenol. Similarly, the dual photoCORM **5** was obtained by converting **4** to the corresponding chloroformate by treating with two equivalents of PNPCl, followed by the addition of DBU to afford **5** in 73% overall yield. Next, the combinatorial photoCORM **8** was synthesized in two steps from compound **6**. First, compound **7** was prepared by carrying out an esterification reaction between compound **6** and chlorambucil (cbl). Finally, compound **7** was subjected to the reaction condition as described for **3** to yield the photoCORM **8** in 71% yield. All the synthesized photoCORMs were characterized by ^1H, ^{13}C NMR, and mass spectral analysis (See Figures S1−S6 in the Supporting Information). We have also provided the purity of photoCORMs **3**, **5**, and **8** by reverse phase-high-performance liquid chromatography (RP-HPLC) (See Figure S7 in the Supporting Information).

Following the successful synthesis of single, dual, and combinatorial photoCORMs, we then turned our attention to the detailed study of the photophysical properties of photoCORMs. Figure 2 shows the normalized absorption and emission spectra of **3**, **5**, and **8** (100 μM) in phosphate-buffered saline (PBS) buffer [pH ∼ 7.4 and 0.5% dimethyl sulfoxide (DMSO)]. The absorption spectrum of **3**, **5**, and **8** exhibits a maximum at 340, 350, and 330 nm, while in the emission spectra, the maximum is centered at 386, 402, and 433 nm, respectively. The results suggest that Stoke's shift for **8** is larger than **3** and **5** due to the existence of the internal charge transfer (ICT) between the carbazole donor and the carbonyl acceptor unit.[30] Absorption, emission maximum, Stoke's shift, and fluorescence quantum yield of **3**, **5**, and **8** are summarized in Table 1. The fluorescence quantum yields (Φ_f) were calculated referenced with DPA (9,10-diphenylanthracene, Φ_f = 0.95 in ethanol) and found to be within the range $0.09 < \Phi_f < 0.24$ for **3**, **5**, and **8** (Table 1).

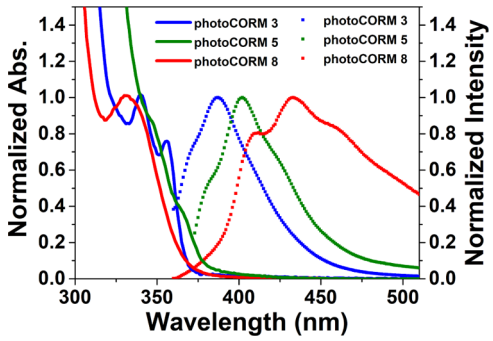

Figure 2. UV absorption (left solid lines) and emission spectra (right dotted lines) of photoCORMs **3**, **5**, and **8**.

Table 1. Synthetic Yields and Photophysical Properties of photoCORMs (3, 5, and 8)

		absorption	fluorescence		
photo CORM	synthetic yield[a] %	λ_{max} (nm)[b]	λ_{max} (nm)[c]	Stoke's shift (nm)[d]	Φ_f[e]
3	81	340	386	46	0.24
5	73	350	402	52	0.16
8	71	330	433	103	0.09

[a]Overall yield. [b]Absorption maximum. [c]Emission maximum. [d]Difference between absorption and emission maximum. [e]Fluorescence quantum yield (error limit within ±5).

Next, the stability of all photoCORMs (**3**, **5**, and **8**) was examined individually in PBS buffer containing 10% fetal bovine serum and cellular thiols (3 mM) [e.g., Cys, Hcys and glutathione (GSH)]. The solution of **3**, **5**, and **8** (100 μM) were ultrasonicated for 10 min to make the solution homogeneous and stored under dark conditions for 72 h at 37 °C. Afterward, the solutions were subjected to the reverse-phase HPLC analysis. Based on the HPLC data, we found that photoCORMs showed good stability (∼96%) in a PBS buffer. However, we observed slightly lower stability for **3** (87%), **5** (92%), and **8** (93%) in the presence of Cys over Hcys and GSH at pH 7.4 (see Figure S8 in the Supporting Information). The above result is reasonable by assuming the higher reactivity of Cys (p*K*a 8.3) compared to HCys (p*K*a 8.6) and GSH (p*K*a 9.0).[31] Overall, the designed photoCORMs were sufficiently stable to be used in biological applications.

Initially, the photouncaging ability of single photoCORM **3** (100 μM, $CDCl_3$) was analyzed under one-photon excitation by irradiation with light of $\lambda \geq 365$ nm using a 125 W medium pressure Hg lamp as the light source and 1 M $CuSO_4$ solution as the UV cut-off filter (Figure 3a). Then, the course of photolysis was examined by ^1H NMR spectroscopy at a regular interval of time (0−20 min). As shown in Figure 3b, the ^1H NMR spectrum at 0 min shows the characteristic peaks at 8.23 ppm (singlet), 7.34 ppm (singlet) corresponding to the aromatic proton (H_a), olefinic proton (H_b) of the single photoCORM **3**, respectively. After 20 min of irradiation, we noticed the complete disappearance of the peaks at 8.23 and 7.34 ppm, which shows the complete decomposition of photoCORM **3**. On the other hand, we observed two new peaks at 9.80 (H_c), 9.05 (H_d) ppm with a gradual increase in peak intensity, indicating the formation of the final photoproduct **3a** [(2,2'-(9-ethyl-9*H*-carbazole-3,6-diyl)bis(2-oxoace-

https://doi.org/10.1021/acs.jmedchem.1c00750
J. Med. Chem. 2022, 65, 1822−1834

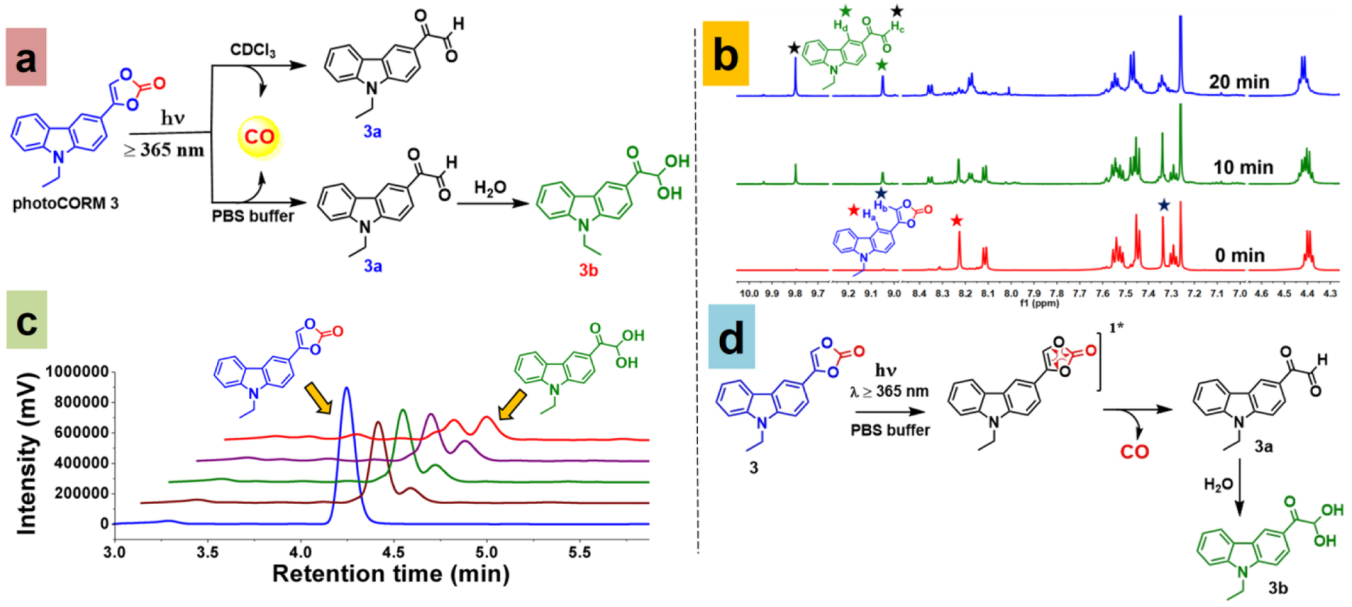

Figure 3. (a) Photolysis of single photoCORM **3** in different solvents like $CDCl_3$ and PBS buffer. (b) ^1H NMR study of single photoCORM **3** (100 μM) in $CDCl_3$ during photolysis. (c) RP-HPLC profile of single photoCORM **3** (1×10^{-4} M) in PBS buffer system (pH = 7.4, 0.5% DMSO) at different time intervals of photolysis ($\lambda \geq 365$ nm). The horizontal axes were offset by 10 s and the vertical axes by 20 mV to facilitate better visualization. (d) Possible photorelease mechanism for single photoCORM **3**.

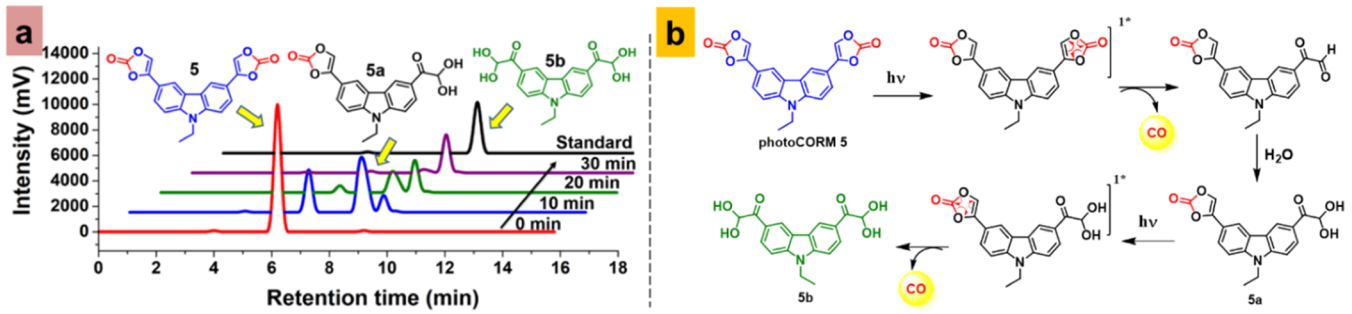

Figure 4. (a) RP-HPLC profile of dual photoCORM **5** (100 μM) in PBS buffer system (pH = 7.4, 0.5% DMSO) at different time intervals of photolysis ($\lambda \geq 365$ nm). The horizontal axes were offset by 10 s and the vertical axes by 20 mV to facilitate better visualization. (b) Possible stepwise photorelease mechanism for dual photoCORM **5**.

taldehyde)] as shown in Figure 3a (see full ^1H NMR spectra Figure S9 in the Supporting Information). Further, the newly formed photoproduct **3a** was characterized by high-resolution mass spectrometry (HRMS) analysis (see Figure S10 in the Supporting Information).

To investigate the photorelease ability of designed photoCORM **3** in a biological system, we performed the photolysis of single photoCORM **3** (100 μM) in a PBS buffer system (pH = 7.4, 0.5% DMSO), and the course of photolysis was monitored by reverse phase-HPLC. From the HPLC analysis, we observed the complete photodecomposition of the **3** and the formation of a photoproduct with an increase in the irradiation time (Figure 3c). Furthermore, we isolated the photoproduct and characterized it by ^1H NMR spectroscopy and HRMS analysis (see Figures S11 and S12 in the Supporting Information). The results suggest that a new photoproduct **3b** [1-(9-ethyl-9*H*-carbazol-3-yl)-2,2-dihydroxyethan-1-one] was formed. In the biological medium, the compound **3a** reacts further with water to form the final photoproduct **3b** (See Figure 3a).[32] The photodecomposition of single photoCORM **3** was further monitored by UV absorption spectroscopy (See Figure S13 in the Supporting Information).

Next, to understand whether the photorelease mechanism occurs from the excited singlet or triplet state, we performed a fluorescence quenching experiment of photoCORM **3** in the presence of benzophenone (a triplet sensitizer), and the result suggested that the photocleavage takes place *via* an excited singlet state (Figure S14 in the Supporting Information). Based on the literature and results of our photolysis experiments, we proposed a possible photorelease mechanism for the single photoCORM **3**, as shown in Figure 3d. Upon irradiation, the excitation of photoCORM **3** to its excited singlet state (S_1) and then it undergoes a cheletropic extrusion of stable CO along with an intermediate photoproduct **3a**, which further reacts with water to form the final photoproduct **3b**.

Next, we examined the photouncaging ability of dual photoCORM **5** (100 μM) in a PBS buffer (pH = 7.4, 0.5% DMSO) by irradiating for 30 min, and the course of the photolysis was monitored by RP-HPLC and ^1H NMR spectroscopy (Figures 4a and S15 in the Supporting Information). Figure 4a shows that as the irradiation time increases, gradual depletion of the peak at t_R = 6.21 min was

https://doi.org/10.1021/acs.jmedchem.1c00750
J. Med. Chem. 2022, 65, 1822−1834

Scheme 2. Sequential Photorelease Mechanism for Combinatorial photoCORM 8

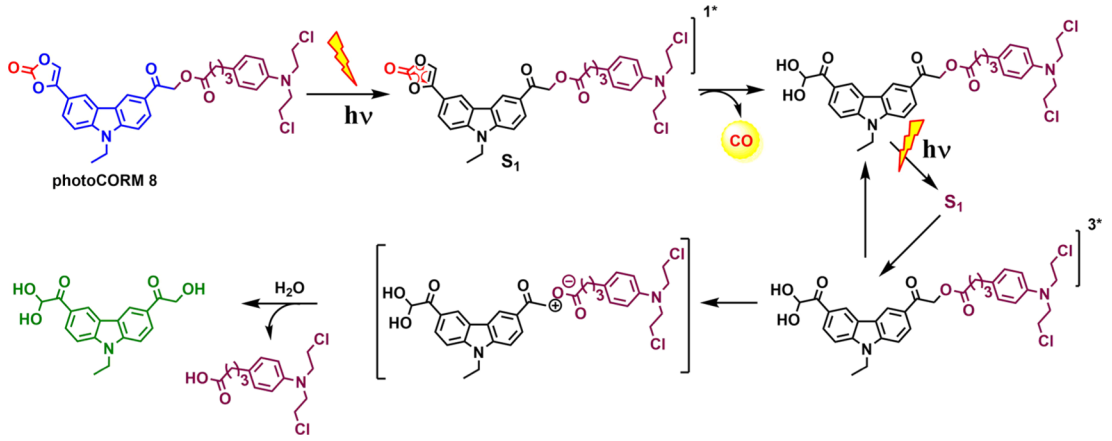

Table 2. Photochemical Properties of photoCORMs (3, 5, and 8)

photoCORM	time of photolysis (min)	% of decomposition[a]	$\varepsilon \times 10^3$ (M^{-1} cm^{-1})[b]	photochemical quantum yield[c] $\Phi_u^{365\ nm}$	ε[d] × $\Phi_u^{365\ nm}$(M^{-1} cm^{-1})	$\delta_a^{730\ nm}$ (GM)[e]	δ_u[f] = $\Phi_u\delta_a$ (GM)$^{730\ nm}$
3	20	93	2.09	0.3	627	n.d[g]	
5	30	89	1.53	0.19	290.7	4.5	0.855
8	60	88	2.16	0.095	203.1	n.d[g]	

[a]% of decomposition based on the formation of the final photoproduct as analyzed by HPLC. [b]Molar absorption coefficient at 365 nm. [c]Photochemical quantum yield for decomposition at $\lambda \geq 365$ nm (error limit ±5%). [d]Action cross-section for one-photon excitation at $\lambda \geq 365$ (error limit ±5%). [e]TPA cross-section (δ_a) at 730 nm. [f]Two photon uncaging cross-section (δ_u) at 730 nm. [g]Not detected.

noted, which indicates photodecomposition of the dual photoCORM **5**. Simultaneously, we also observed a gradual increment of two new peaks at t_R = 8.05 and 8.82 min, corresponding to the single side decomposed intermediate **5a** and the final photoproduct **5b**, respectively (Figure 4b). Continuing photolysis for up to 30 min, we observed the complete decomposition of **5** and **5a** to give the final photoproduct **5b**. The photodecomposition of dual photoCORM **5** was also supported by UV absorption spectroscopy (See Figure S16 in the Supporting Information).

Based on the HPLC analysis and the ^{1}H NMR study of the photolysate of dual photoCORM **5**, it can be evident that the photouncaging of CO from photoCORM **5** proceeds in a step wise pathway following the similar mechanism as was in the case of single photoCORM **3** (Figure 4b). To validate the proposed stepwise mechanism, the photolysis mixture of dual photoCORM **5** (after 10 min of irradiation) was subjected to HRMS analysis. It was found that the possible intermediate **5a** along with the final photoproduct **5b** was present in the reaction mixture, and the final photoproduct **5b** was isolated and characterized by ^{1}H NMR spectroscopy and HRMS analysis (see Figures S17 and S18 in the Supporting Information).

Lastly, the photorelease ability of combinatorial photoCORM **8** (100 μM) in PBS buffer was examined (pH = 7.4 and 0.5% DMSO) by irradiating for 60 min, and the course of the photolysis was followed by RP-HPLC (Figure S19 in the Supporting Information). The photorelease profile showed the sequential uncaging of active molecules (CO and drug, i.e., chlorambucil) as shown in Scheme 2. Based on HPLC data, it was evident that the fast uncaging of CO compared to the drug. Then, the percentage of the released drug was calculated by injecting an authentic sample and found to be 87% (see Figure S20 in the Supporting Information) and the rate of photorelease found to be 2.483×10^{-2} s^{-1}. We also monitored the course of photodecomposition of photoCORM **8** by UV absorption spectroscopy (See Figure S21 in the Supporting Information). Furthermore, the photochemical quantum yields (Φ_p) of all the photoCORMs **3**, **5**, and **8** were calculated using potassium ferrioxalate as an actinometer (Table 2).[33]

After one-photon excitation, we intended to determine the two-photon uncaging ability of the designed photoCORMs (3, 5, and 8) because it will enable spatio-temporal uncaging with a lower phototoxicity and deep-tissue penetration ability. To determine the two-photon absorption (TPA) cross-section (δ_a) for photoCORMs (**3**, **5**, and **8**), we performed the nonlinear optical measurements using the open aperture (OA) z-scan technique with a laser pulse of 150 fs with 1 kHz repetition rate at a wavelength of 730 nm. Among the designed photoCORMs, dual photoCORM **5** only showed a positive TPA cross-section (δ_a), probably due to the higher symmetry of photoCORM **5**, and it was calculated to be 4.5 GM (1 GM = 10^{-50} cm^4 s/photon) at 730 nm (See Figure S22). Then, the two-photon uncaging cross-section (δ_u) for **5** was calculated to be 0.855 GM using the equation $\delta_u = \delta_a\Phi_u$, where Φ_u is the quantum yield of the uncaging reaction and the result was shown in Table 2. The result suggests that the δ_u value of **5** was more significant than the limit of 0.1 GM reported to ensure suitability for biological applications.

Next, we also performed two-photon photolysis of dual photoCORM **5** with a laser of 100 fs pulse at the 1 kHz repetition rate at the wavelength of 730 nm for 30 min, and the photolysis was followed by RP-HPLC. From the HPLC peak area compared to the injected authentic sample, we found that 37% of the decomposition of photoCORM **5** occurred in 30 min of irradiation (see Figure S23 in Supporting Information).

Next, we aimed to detect and quantify the CO release from the designed photoCORMs. For this purpose, we synthesized

https://doi.org/10.1021/acs.jmedchem.1c00750
J. Med. Chem. 2022, 65, 1822−1834

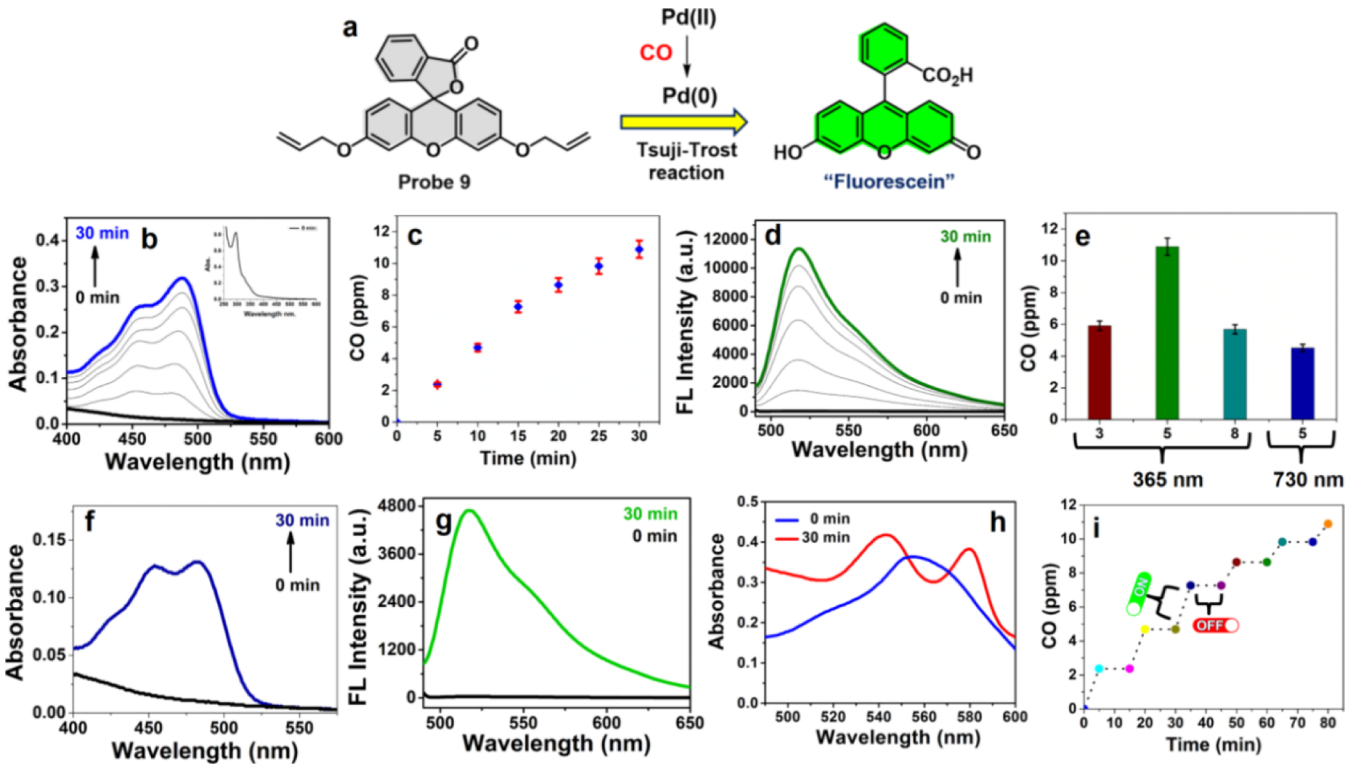

Figure 5. (a) Proposed CO detection mechanism. (b) Absorption spectra recorded during photolysis of photoCORM **5** in PBS buffer (pH = 7.4 and 0.5% DMSO) in the presence of probe **9** and $PdCl_2$ at regular time intervals ($\lambda \geq 365$ nm). (c) Time-dependent CO release from photoCORM **5** in parts per million (ppm). (d) Emission spectra recorded during photolysis of photoCORM **5** in the presence of probe **9** and $PdCl_2$, Excitation wavelength: 480 nm. (e) Comparison of the amount of CO release from photoCORMs **3**, **5**, and **8** at $\lambda \geq 365$ nm and photoCORM **5** at 730 nm for 30 min of irradiation. (f) Absorption and (g) emission spectra recorded during photolysis of photoCORM **5** in the presence of probe **9** and $PdCl_2$ at 730 nm for 30 min. (h) CO detection from photoCORM **5** by myoglobin assay. (i) Progress of the CO release from photoCORM **5** under dark and light conditions (OFF indicates the end of light irradiation and ON indicates the start of light irradiation. Final concentrations of photoCORMs (500 μM) in PBS buffer (pH = 7.4 and 0.5% DMSO), probe **9** (100 μM) and $PdCl_2$ (200 μM).

the well-known photostable fluorescein-based turn-on fluorescent probe **9** as described in the literature.[34]

To confirm the CO release from the photoCORM **5**, we investigated the response of probe **9** in the presence of $PdCl_2$ (Figure 5a). As shown in Figure 5b, we recorded the change in the absorption spectrum of the photolysis mixture (500 μM photoCORM **5** + 100 μM probe **9** + 200 μM $PdCl_2$) in a PBS buffer (pH 7.4, with 0.5% DMSO) at different time intervals. Figure 5b shows a strong absorption band at 295 nm, which corresponds to the absorption of probe **9** at 0 min. With a gradual increase in the irradiation time using the light of $\lambda \geq$ 365 nm, we observed a new absorption band at 488 nm with increasing intensity. A remarkable red shift in the absorption peak from 290 to 488 nm was apparently due to the formation of fluorescein by the result of the Tsuji−Trost[34] type of reaction between the probe and CO in the presence of $PdCl_2$, confirming the ability of **5** to release CO upon photoirradiation. Then, we quantified the amount of CO released at different time intervals (Figure 5c) based on the calibration curve obtained from the commercially available standard CO precursor, CORM-3 (see Figure S24 in the Supporting Information).

Furthermore, the same probe **9** was also used to monitor CO release by fluorescence spectroscopy qualitatively. Figure 5d shows a gradual increase in fluorescence intensity at 518 nm with a gradual increase in exposure time. Next, we also carried out detection and quantification of CO release from the single and combinatorial photoCORMs by both absorption and fluorescence spectroscopy (see Figures S25 and S26 in the Supporting Information). Overall, the results suggest that dual photoCORM **5** was able to release a quantitative amount of CO, around 12 ppm at 500 μM after 30 min of photolysis with the light of $\lambda \geq$ 365 nm, compared to the single (5.9 ppm) and combinatorial (5.7 ppm) photoCORMs (Figure 5e).

Next, the two-photon uncaging of CO from dual photoCORM **5** was monitored using the same turn-on fluorescent probe **9**, except herein, we used a laser of 100 fs pulse at the 1 kHz repetition rate at the wavelength of 730 nm for 30 min. Figure 5f,g shows the quantitative and qualitative detection of CO release from photoCORM **5** under two-photon excitation, respectively. The amount of CO release from photoCORM **5** was found to be 4.5 ppm at 730 nm (Figure 5e). The efficient CO uncaging ability of dual photoCORM **5** in the NIR region prompted us to explore its possibilities as a competent CO donor for the tumor regression *in vivo*. Further, to provide direct evidence of CO release by photoCORMs, the standard myoglobin assay was performed. It was shown that incubation of deoxy-myoglobin (MbFe(II)) (500 μM, pH = 7.4) with the photolysis mixture of dual photoCORM **5** (500 μM) in PBS buffer (pH = 7.4 and 0.5% DMSO) produces carbonmonoxy-myoglobin (MbCO) as evident by the change in absorbance. As shown in Figures 5h and S27 in the Supporting Information, the intensity of the absorption maximum in the Q band region of MbFe(II) decreases at 557 nm, while at 540 and 577 nm, two new bands appeared, which correspond to the formation of MbCO.

https://doi.org/10.1021/acs.jmedchem.1c00750
J. Med. Chem. 2022, 65, 1822−1834

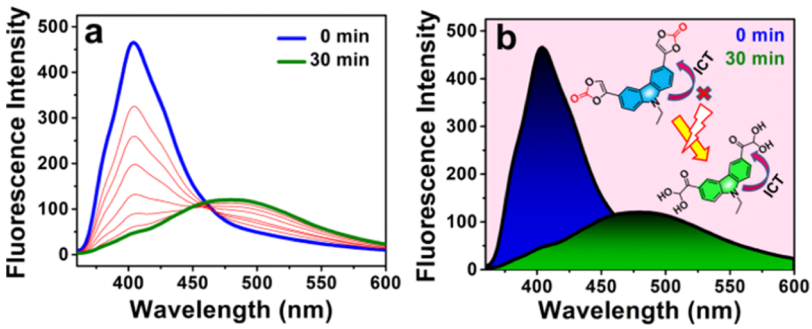

Figure 6. (a) Emission spectra of dual photoCORM **5** (100 μM) in PBS buffer (pH = 7.4 and 0.5% DMSO) measured during photolysis at different interval of time (0−30 min). (b) Comparison of fluorescent spectral profile at 0 and 30 min of light irradiation. Excitation wavelength: 350 nm.

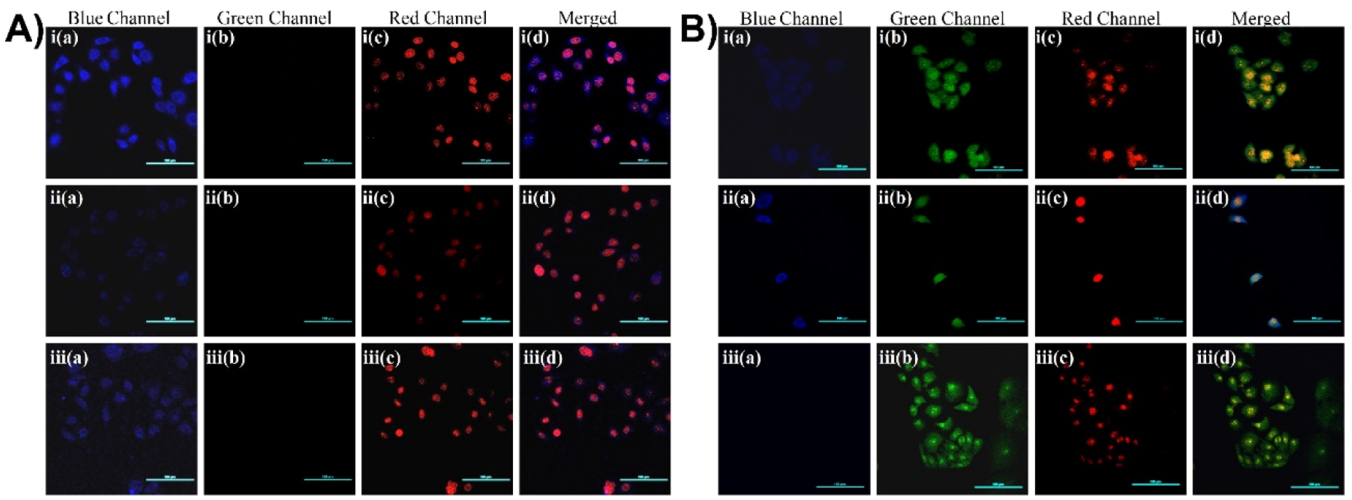

Figure 7. CLSM images of B16F10 cells incubated with photoCORMs **3** (i), **5** (ii), and **8** (iii), respectively, for 4 h: (A) before photoirradiation and (B) after photoirradiation for 5 min ($\lambda \geq 365$ nm). Cell nuclei were marked with propidium iodide (red). Scale bar = 100 μm.

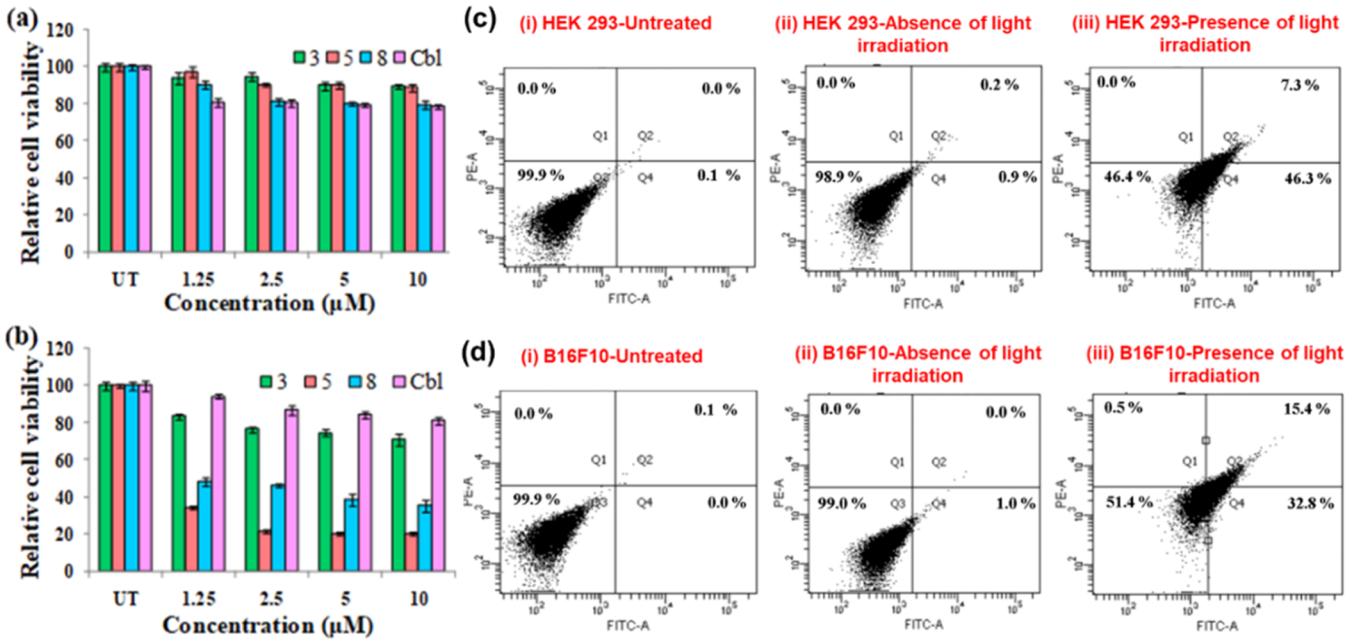

Figure 8. photoCORM **5** upon light irradiation induces the apoptosis leads to enhanced cytotoxicity in B16F10 cells. Cell viability assays of photoCORMs **3**, **5**, and **8** on B16F10 cells: (a) without irradiation, (b) with irradiation (5 min). Values are represented as means ± standard deviations of triplicates. Apoptosis detection assay of photoCORM **5** for 24 h (c) HEK 293 and (d) B16F10 cells. The percentage of apoptosis was estimated using Annexin−V binding assay.

https://doi.org/10.1021/acs.jmedchem.1c00750
J. Med. Chem. 2022, 65, 1822−1834

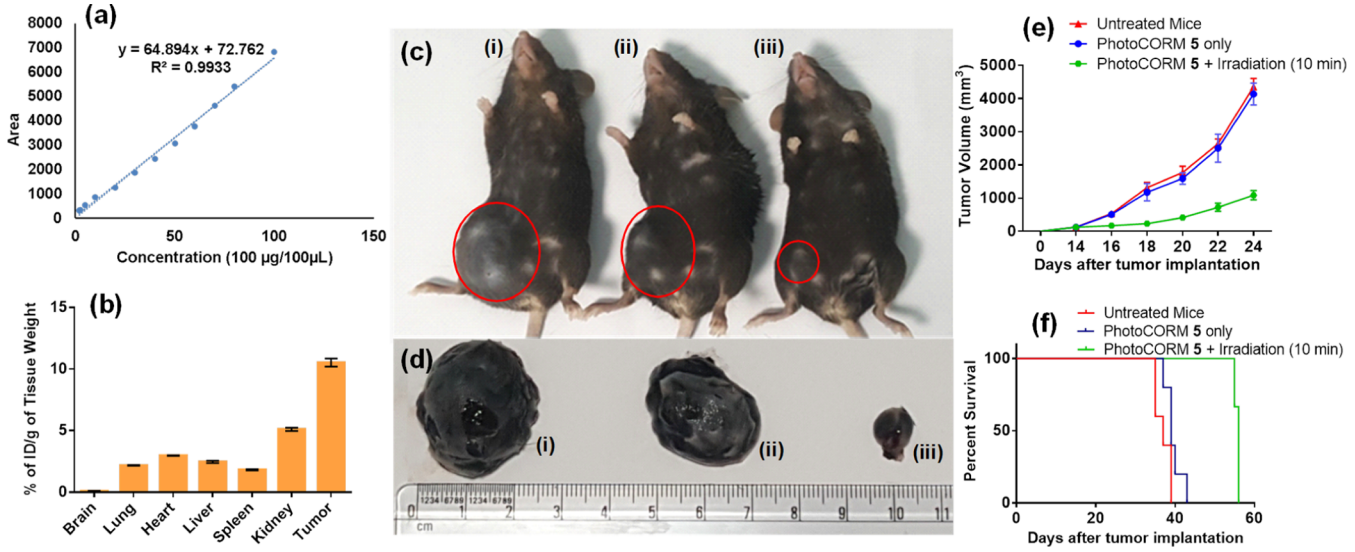

Figure 9. *In vivo* biodistribution profile and tumor regression study on C57BL/6J mice model using photoCORM **5**: (a) calibration curve representing the fluorescent plot area of photoCORM **5** in different concentration in ^{i}PrOH, (b) relative biodistribution of compound **5**, (c) representative tumor bearing mice: (i) UT, (ii) treated with photoCORM **5** only and (iii) treated with compound **5** + 10 min of light irradiation (d) representative images of isolated tumors in each group: (i) UT mice, (ii) mice treated with photoCORM **5** only and (iii) mice treated with photoCORM **5** + 10 min of light irradiation (e) Relative tumor growth inhibition upon i.v. injected with photoCORM **5**, (f) overall survivability of the mice groups were monitored after the final intravenous injection on day 24 post-tumor inoculation.

To better understand the precise control over the CO release by light, CO release from dual photoCORM **5** was monitored periodically by switching the light source on and off. Figure 5i shows that CO release was stopped when the light source was turned off, which clears that only an external stimulus, such as light, is responsible for the release of CO.

To evaluate the real-time monitoring ability of the designed photoCORMs, we excited the photoCORM **5** at 350 nm. At 0 min, it showed a blue-emission band at λ_{max} =404 nm corresponds to photoCORM **5** (Figure 6). As the irradiation time gradually increases, the blue emission band at λ_{max} = 404 nm gradually decreases with a concomitant increase in the new green emission band at λ_{max} = 485 nm. After 30 min of irradiation, we observed complete quenching of the band at λ_{max} = 404 nm. In contrast, the maximum intensity was observed for the band at λ_{max} = 485 nm, and the above observation can be ascribed to the ICT transition existing between the carbazole donor and carbonyl acceptor moiety of the newly formed photoproduct **5b**. A well-defined isosbestic point at 460 nm indicates that the existence of an equilibrium between **5** and **5b** upon irradiation. Next, the real-time monitoring ability of the single and combinatorial photoCORMs was also investigated (Figures S28 and S29 in the Supporting Information). Also, the absorption and emission spectra of photoproducts **3b** and **5b** were recorded independently (see Figures S30 and S31 in the Supporting Information), and it was confirmed that the distinct fluorescence color change was due to the uncaging process. Thus, the course of CO release on account of photoirradiation can be monitored in real-time by observing the change in color from blue to green.

To investigate the cellular uptake and real-time monitoring of CO uncaging of photoCORMs **3**, **5** and **8**, cellular imaging studies were performed on cancerous B16F10 cells. Cells were incubated with compounds **3**, **5**, and **8** separately for 4 h at 37 °C. The cells showed a strong blue fluorescence (Figure 7A. i(a), ii(a), and iii (a)) under a confocal laser scanning microscope (CLSM) imaging upon excitation at 330 nm, which reveals that the corresponding photoCORMs were readily internalized by the cells. To demonstrate the real-time monitoring ability of photoCORMs **3**, **5**, and **8**, confocal microscopy images were recorded post irradiation using the light of $\lambda \geq 365$ nm. After light irradiation for 5 min, we observed a complete fluorescence color change from blue to green [Figure 7B. i(b), ii(b), and iii (b)], suggesting the complete uncaging of active molecules (CO and cbl) from photoCORMs **3**, **5** and **8**.

Further, the *in vitro* cellular toxicity was determined by MTT based cell viability assay on B16F10 cells, before and after photolysis (Figure 8a,b, respectively). Briefly, two sets of cells were incubated with compounds **3**, **5**, **8** and the commercially available anticancer drug cbl in different concentrations (1.25, 2.50, 5, and 10 μM) for 72 h, and one set of cells was subjected to photolysis after 6 h of post treatment using the light of $\lambda \geq$ 365 nm for 5 min, then allowed to incubate for 72 h. The percentages of cell viability versus concentration of compounds before and after photolysis are presented in Figure 8a,b. From the results, it is evident that after photolysis, single photoCORM **3** showed 70% cell viability by releasing one equiv of CO, dual photoCORM **5** showed 20% cell viability by the release of two equiv of CO, and photoCORM **8** showed 35% cell viability by releasing one equiv of CO and one equiv of cbl. In contrast, free cbl showed more than 80% of cell viability at the concentration of 10 μM. It can also be noted that on photoirradiation, the photoCORM **5** showed 21% of cell viability even at a concentration of 2.5 μM. Thus, it is evident that the dual photoCORM **5** possesses potent anticancer activity upon photoirradiation compared to cbl, single photoCORM **3** and combinatorial photoCORM **8**.

In addition, careful analysis of MTT data showed that free cbl and photoCORM **3** having more than 80 and 70% of cell viability upon photoirradiation, respectively, while the photoCORM **8**, which could release a cocktail of both CO and cbl one equivalent of each on photoirradiation, is showing lower

https://doi.org/10.1021/acs.jmedchem.1c00750
J. Med. Chem. 2022, 65, 1822−1834

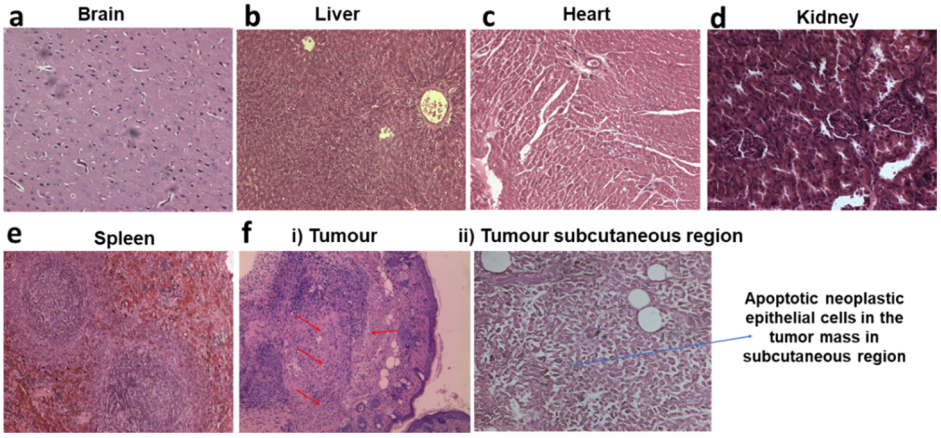

Figure 10. H&E staining of photoCORM **5** treated mice organs and tumor tissues (a) brain, (b) liver, (c) heart, (d) kidney, (e) spleen, and (f) (i) tumor; red arrows indicate that large area of apoptosis in tumor mass was replaced with fibrous tissues and (ii) tumor subcutaneous region.

cell viability of 35%. Therefore, it can be concluded that the released CO is enhancing the therapeutic efficacy of the chemotherapeutic drug cbl. This result is further supporting the observation by the BIDMC team on their pioneering work on CO-based chemotherapy.[4]

To investigate whether the photoCORM **5** induces apoptosis or not, the non-cancerous HEK293 and cancerous B16F10 cells were treated with photoCORM **5**. The apoptosis levels were estimated using an annexin-V binding assay, photoCORM **5** followed by light irradiation induced the late apoptosis in cancer cells (15.4%) by two-fold compared to non-cancerous cells (7.3%). The photoCORM **5**-treated cancerous and non-cancerous cells followed by light irradiation-induced apoptosis within 24 h, but without light-irradiation the cells were not significantly showed apoptosis, further proving that the "CO" release was important in enhancing the apoptosis levels in the cells. The photoCORM **5** untreated (UT) cells (Figure 8c(i),d(i)) upon light irradiation did not show apoptosis (Figure 8c,d). Based on these results, it was confirmed that the photoCORM **5** enhances the selective cytotoxicity upon light irradiation.

Further, to evaluate the tumor selective biodistribution profile of photoCORM **5**, the orthotopic murine melanoma model was established. Initially, 250 μL of Hank's buffer salt solution (HBSS) containing B16F10 cells (2×10^5) were subcutaneously injected in the right flank of six to eight weeks old C57BL/6 female mice ($n = 3$, weights of each group ~22−25 g). After 18 days of post tumor implementation (when tumor volume reached ~1500 mm^3), one dose of photoCORM **5** (0.4 mg/kg BW of mice) was administered intravenously to the mice. After 24 h of post-injection, vital organs from treated mice were isolated to evaluate the biodistribution of photoCORM **5** in different tissues, including the tumor. Acidified isopropanol (0.5 mL) was added to the tissue and tumor samples and homogenized with a mechanical homogenizer for 60 s at 5000 beats/minute. All tissue samples were maintained at an ice cold condition before and after the homogenization in the dark. Homogenized samples were incubated overnight in acidified isopropanol (90 percentage isopropanol, 75 mM hydrochloric acid, 10 percentage water) at 4 °C. Then, the samples were vortexed and centrifuged (14 000 rpm) for 10 min at 4 °C; further, the supernatant (100 μL per well) was plated onto a 96-well plate in triplicates. Concentrations of the photoCORM **5** in isolated tissue extracts were estimated by comparing the fluorescence peak area of tissues extracts with the standard calibration curve of concentration of photoCORM **5** vs An emission peak area plot (Figure 9a) (The fluorescence of tissue extracts from UT control mice was used to rectify the background fluorescence of tissue extracts). The biodistribution experiment revealed a profound accumulation of photoCORM **5** on the tumor site, followed by kidney, heart, liver, lung, and spleen (Figure 9b).

The tumor selective biodistribution profile of photoCORM **5** (Figure 9b) and its potent *in vitro* anticancer efficacy (Figure 8b) prompted us to examine its therapeutic efficacy in *in vivo* settings to inhibit the established melanoma tumor mice model. The melanoma tumor (established by subcutaneous injections of 2×10^5 B16F10 cells in HBSS into the right flanks of mice on day zero) bearing mice were arbitrarily distributed ($n = 5$) into three groups. The divided three groups include group I: UT mice, group II: injected with photoCORM **5** (0.4 mg/kg BW of mice), and group III: injected with photoCORM **5** (0.4 mg/kg BW of mice, group III) + light irradiation (using a laser source of 730 nm) at the tumor site (10 min) after 24 h of each injection starting from day 14, 16, 18, 20, 22, and 24. Group I was intravenously administered (alternative days) with 5% aqueous glucose, whereas Group II and III were intravenously administered (alternative days, total six doses) with photoCORM **5** (0.4 mg/kg BW of mice) in every alternative day. Tumor volumes were estimated using slide calipers for up to 24 days. Notably, the tumor growth was significantly less in group III than in other groups (Figure 9c−e). On day 25th of tumor inoculation, one mouse from each group was sacrificed, and tumors were harvested, which clearly showed profound regression of the tumor in group III mice. Most importantly, the overall survivability benefit was ~57% higher in mice of group III compared to that of the control mice of group I (Figure 9f).

To validate the *in vivo* toxicity of photoCORM **5**, it was investigated on the C57BL/6J mouse tumor model. ~4−6 weeks old B16F10 tumor bearing C57BL/6J mice were intravenously (i.v.) injected with photoCORM **5** as mentioned earlier in the tumor inhibition study (6 treatment doses). In addition, in a control experiment, the mice were i.v. injected with HBSS for every alternate day up to 12 days. The weight and movement of all mice were monitored every day. In the treatment period of photoCORM **5**, it was found that there is no significant difference in terms of body weights and

https://doi.org/10.1021/acs.jmedchem.1c00750
J. Med. Chem. 2022, 65, 1822−1834

movement of the mice compared to the remaining treated mice and in the mice used for the control experiment (data not shown), which undoubtedly demonstrated that the corresponding six doses were in a bearable range for all mice. Upon completion of the treatment, the mice were euthanized and the tissues of vital organs (five), that is, liver, heart, kidney, lung, spleen, and tumor were isolated from photoCORM **5** treated group and subjected to hematoxylin and eosin (H&E) staining, it clearly demonstrated that there is no visible necrosis of the tissue in all five vital organs (Figure 10) and showed the photoCORM **5** treated tumor tissue necrosis. Therefore, the *in vivo* toxicity studies evidently showed that the photoCORM **5** could be considered as non-toxic for further applications.

CONCLUSIONS

In summary, we demonstrated the design and synthesis of three new metal-free photoCORMs (single, dual, and combinatorial models) based on a carbazole fused 1,3-dioxol-2-one moiety for the release of one equiv of CO, two equiv of CO, and one equiv of CO and one equiv of the anticancer drug upon excitation, respectively. Next, we examined the detailed photophysical and photochemical properties of all the photoCORMs under one- and two-photon excitation. The photorelease mechanism for dual CO release of photoCORM **5** proceed through a stepwise manner, it was supported by ^{1}H NMR and RP-HPLC experiments. Interestingly, the dual photoCORM **5** showed a good two-photon uncaging cross section (δ_u) for CO release in the "phototherapeutic window". Further, we confirmed that the dual photoCORM **5** could release the quantitative amount of CO at a lower dosage compared to single and combinatorial models using a fluorescein-based "turn on" probe as well as standard myoglobin assay. The unique feature of the designed photoCORMs was that they could show CO uncaging real-time monitoring through the non-invasive approach of fluorescent color change from blue to green. The *in vitro* cellular uptake studies of photoCORMs in cancerous B16F10 cells manifested that efficient cellular internalization and real-time monitoring ability of CO release utilizing non-invasive fluorescence color change approach from blue to green at a cellular level. The *in vitro* cytotoxicity results based on B16F10 melanoma cell line evident that photoCORM **5**, which releases two equiv of CO upon irradiation, was the most promising in killing B16F10 melanoma cells compared to the single and combinatorial photoCORMs. The cytotoxicity of photoCORM **5** was further supported by the apoptosis study. Our results also reveal that CO can accelerate the effectiveness of the well-known anticancer drug (chlorambucil). Moreover, the *in vivo* assessment of the photoCORM **5** on an established murine melanoma tumor (C57BL/6J mice model) demonstrated that the mice injected with photoCORM **5** (total 6 doses), followed by irradiation at 730 nm, showed a significant regression in tumor volume, led to substantial (>50%) enhancement in the overall survivability of the tumor-bearing mice compared to that of the overall survivability of UT tumor-bearing mice. In addition, the *in vivo* toxicology studies based on the H&E staining clearly show that photoCORM **5** could be considered as non-toxic. Therefore, we anticipate that the superior features of the developed dual photoCORM **5** can be used in ongoing cancer, vascular disease research and help to better understand the biological benefits of CO.

EXPERIMENTAL SECTION

General Information. Commercially available anhydrous solvents dichloromethane (DCM), dimethylformamide (DMF), ethyl acetate (EA), petroleum ether, and other chemicals were used without further purification. Acetonitrile (ACN) and DCM were distilled from CaH_2 before use. NMR spectra were recorded on a 400 and 600 MHz instrument. ^{1}H NMR chemical shifts were referenced to the tetramethylsilane signal (0 ppm), ^{13}C NMR chemical shifts were referenced to the solvent resonance (77.23 ppm, Chloroform-*d* ($CDCl_3$)). Chemical shifts (δ) are reported in ppm, and spin−spin coupling constants (J) are given in Hz. Below abbreviations were used to explain multiplicities: s = singlet, d = doublet, t = triplet, q = quadruplet, m = multiplet. UV/vis absorption spectra were recorded on a Shimadzu UV-2450 UV/vis spectrophotometer, and fluorescence spectra were recorded on a Hitachi F-7000 fluorescence spectrophotometer. HRMS were recorded on ESI-TOF (electrospray ionization-time-of-flight). Photolysis was carried out using a 125 W medium pressure mercury lamp. Chromatographic purification was carried out with a 60−120 mesh silica gel. We have determined the purity of the synthesized photoCORMs by RP-HPLC using a mobile phase, a gradient of ACN/water (water containing 0.1% trifluoroacetic acid) (phase 1/phase 2). Methods were performed with a flow rate of 1.0 mL/min. Compounds were detected at λ = 254 nm, and target compounds were >95% pure. FITC-labeled annexin-V and propidium iodide (PI) were purchased from Sigma, St. Louis, USA.

*Synthesis of Compounds **1**, **4**, and **6**.* Synthetic procedure for the compounds **1**, **4**, and **6** was described in the literature.[28,29]

*Synthesis of 4-(9-Ethyl-9H-carbazol-3-yl)-1,3-dioxol-2-one (**3**).* To a solution of **1** (0.200 g, 0.78 mmol) and Et_3N (0.119 g, 1.18 mmol, 1.5 equiv) in dry DCM (20 mL), a solution of 4-nitrophenyl chloroformate (0.190 g, 0.94 mmol, 1.2 equiv) in DCM (20 mL) was added dropwise at 0 °C. After stirring at room temperature for 30 min, the reaction progress checked by the TLC and the solvent was concentrated to give the product **2** as a yellow crystalline solid. Then, in situ reaction of **2** in the presence of DBU (0.36 g, 2.37 mmol, 3 equiv) in dry DMF (2 mL) and then stirred at room temperature for 2 h. Upon completion of the reaction, it was extracted with EA and washed with 1 M $NaHCO_3$, water, and saturated NaCl solution. The organic layer was dried over Na_2SO_4 and concentrated under reduced pressure and then the crude product was purified by column chromatography using 10% EtOAc in pet ether to give the product as a white solid (0.178 g, 81%). ^{1}H NMR (600 MHz, $CDCl_3$): δ 8.23 (s, 1H), 8.11 (d, J = 7.7 Hz, 1H), 7.59−7.48 (m, 2H), 7.45 (d, J = 8.4 Hz, 2H), 7.34 (s, 1H), 7.29 (t, J = 7.4 Hz, 1H), 4.39 (q, J = 7.1 Hz, 2H), 1.46 (t, J = 7.3 Hz, 3H). ^{13}C{^{1}H} NMR (151 MHz, $CDCl_3$): δ 153.3, 145.0, 140.6, 126.8, 123.4, 123.4, 123.1, 122.7, 121.7, 121.7, 120.9, 116.8, 115.3, 109.2, 109.1, 38.0, 14.0. HRMS (ESI$^+$): calcd for $C_{17}H_{13}NO_3$ [M + H]$^+$, 280.0974; found, 280.0970. HPLC: t_R = 4.802 min, purity > 95%.

*Synthesis of 4,4′-(9-Ethyl-9H-carbazole-3,6-diyl)bis(1,3-dioxol-2-one) (**5**).* To a solution of **4** (0.200 g, 0.64 mmol) and Et_3N (0.195 g, 1.92 mmol, 3 equiv) in dry DCM (20 mL), solution of 4-nitrophenyl chloroformate (0.310 g, 1.54 mmol, 2.4 equiv) in DCM (20 mL) was added a dropwise at 0 °C. After stirring at room temperature for 30 min, the reaction progress was checked by the TLC and the solvent was concentrated to give the product as a yellow crystalline solid. Then, in situ reaction of **5** in the presence of DBU (0.586 g, 0.642 mmol, 6 equiv) in dry DMF (2 mL) and then stirred at room temperature for 4 h. Upon completion of the reaction, it was extracted with EA and washed with water and saturated NaCl solution. The organic layer was dried over Na_2SO_4 and it was concentrated under reduced pressure and then the crude product was purified by column chromatography using 30% EtOAc in pet ether to gives the product as a light-yellow solid (0.165 g, 71%). ^{1}H NMR (600 MHz, DMSO-d_6): δ 8.51 (s, 2H), 8.26 (s, 2H), 7.80 (d, J = 8.6 Hz, 2H), 7.72 (d, J = 8.6 Hz, 2H), 4.52 (q, J = 7.2 Hz, 2H), 1.34 (t, J = 7.1 Hz, 3H). ^{13}C{^{1}H} NMR (151 MHz, DMSO-d_6): δ 153.1, 144.0, 140.7, 125.7, 122.6, 122.5, 117.0, 116.4, 110.9, 37.9, 14.3. HRMS (ESI$^+$): calcd for

https://doi.org/10.1021/acs.jmedchem.1c00750
J. Med. Chem. 2022, 65, 1822−1834

$C_{20}H_{13}NO_6$ $[M + H]^+$, 364.0821; found: 364.0820. HPLC: t_R = 4.257 min, purity > 95%.

*Synthesis of 2-(9-Ethyl-6-(2-oxo-1,3-dioxol-4-yl)-9H-carbazol-3-yl)-2-oxoethyl 4-(4-(bis(2-chloroethyl)amino)phenyl)butanoate (**8**).* The reaction of **6** (0.150 g, 0.40 mmol) and chlorambucil (0.121 g, 0.40 mmol) in dry DMF in the presence of K_2CO_3 (0.066 g, 0.48 mmol), stirred at room temperature over a period of 30 min. Upon completion of the reaction, it was extracted with EA and then the crude conjugate was purified by column chromatography using 30% EtOAc in pet ether to give the product **7** as a light-yellow solid (0.217 g, 91%). To a solution of **7** (0.200 g, 0.335 mmol) and Et_3N (0.050 g, 0.502 mmol) in dry DCM (20 mL) at 0 °C, a solution of 4-nitrophenyl chloroformate (0.08 g, 0.402 mmol) in DCM (20 mL) was added dropwise. After stirring at room temperature for 30 min, the solvent was concentrated to give the product as yellow crystals and then we carried out in situ reaction in the presence of DBU (0.152 g, 1.004 mmol, 3 equiv) in dry DMF (2 mL) and then stirred at room temperature overnight. After completion of the reaction, it was extracted with EA and washed with water and saturated NaCl solution and dried over Na_2SO_4. The solvent was concentrated by rotary evaporation and then the crude product was purified by column chromatography using 30% EtOAc in pet ether to give the product as a light-yellow solid (0.162 g, 78%). ^{1}H NMR (600 MHz, $CDCl_3$): δ 8.67 (s, 1H), 8.22 (s, 1H), 8.11 (d, J = 9.9 Hz, 1H), 7.61 (d, J = 8.5 Hz, 1H), 7.47 (dd, J = 18.2, 8.6 Hz, 2H), 7.37 (s, 1H), 7.11 (d, J = 8.5 Hz, 2H), 6.63 (d, J = 8.6 Hz, 2H), 5.49 (s, 2H), 4.40 (q, J = 7.2 Hz, 2H), 3.70 (t, J = 7.1 Hz, 4H), 3.62 (t, J = 7.0 Hz, 4H), 2.65 (t, J = 7.5 Hz, 2H), 2.55 (t, J = 7.4 Hz, 2H), 2.10−1.95 (m, 2H), 1.47 (t, J = 7.3 Hz, 3H). ^{13}C{^{1}H} NMR (151 MHz, $CDCl_3$): δ 191.5, 173.4, 153.0, 144.5, 144.4, 143.6, 141.3, 130.0, 126.6, 126.5, 123.7, 123.5, 122.7, 122.5, 121.6, 116.9, 116.8, 112.4, 110.0, 109.1, 66.1, 53.8, 40.7, 38.3, 34.1, 33.5, 27.0, 14.0. HRMS (ESI$^+$) calcd for $C_{33}H_{32}Cl_2N_2O_6$ $[M + H]^+$, 623.1716; found, 623.1713. HPLC: t_R = 6.415 min, purity > 95%.

*Synthesis of 3′,6′-Bis(allyloxy)-3H-spiro[isobenzofuran-1,9′-xanthen]-3-one (Probe **9**).* Synthetic procedure for the probe **9** was described in the literature.[34]

Experimental Procedure for *In Vitro* and *In Vivo* Applications. *Cellular Uptake Study of the Designed photoCORMs Using Confocal Microscopy.* The degrees of cellular internalization and real-time monitoring ability of the designed photoCORMs (**3**, **5**, and **8**) in cancer cells were studied qualitatively by confocal microscopy. Briefly, the cancerous B16F10 cells were seeded (1×10^5 cells/mL) in a 35 mm cover glass with 1 mL of growth medium content complete Dulbecco's modified eagle's medium (DMEM) with 10% of fetal bovine serum (FBS) incubated for overnight at 37 °C in a 5% CO_2 incubator, then cells were rinsed (3 × 1 mL) with 1× PBS. One set of cells was incubated with the photoCORMs (20 μM) for 4 h at 37 °C in a 5% CO_2 incubator. Further, cells were rinsed (3 × 1 mL) with 1× PBS then fixed with 4 percentage of paraformaldehyde, and cell nuclei were stained with propidium iodide and fixed with 4% paraformaldehyde. Mount on coverslip onto a glass slide and images were recorded by confocal microscopy (Nikon Ti Eclipse).

Another set of cells were incubated with the photoCORMs (20 μM) for 4 h at 37 °C in a 5% CO_2 incubator. After incubation, the cells were light irradiated for 5 min with a medium pressure Hg lamp (125 W) as $\lambda \geq 365$ nm UV light source and 1 M $CuSO_4$ solution as a UV cut-off filter and further incubated for 4 h. Then, the cells were washed (3 × 1 mL) with 1× PBS then and cell nuclei were stained with propidium iodide and fixed with 4% paraformaldehyde. Mount on coverslip onto a glass slide and images were recorded by Nikon Ti Eclipse confocal microscopy.

Cytotoxicity of photoCORMs without Photolysis. The cytotoxicity of the designed photoCORMs (**3**, **5**, and **8**) and free drug chlorambucil was estimated with an MTT assay. B16F10 cells were plated (5000 cells per well) in 96 well plate, after 24 h of post-incubation, cells were incubated with the different concentrations such as UT and 1.25, 2.5, 5, and 10 μM of photoCORMs (3, 5, and 8) and chlorambucil in N-(2-hydroxyethyl)piperazine-N′-ethanesulfonic acid (HEPES) buffer containing 0.5% DMSO was added and incubated at 37 °C in a 5% CO_2 incubator for 72 h. Further, 0.4 mg/mL MTT containing DMEM was added to the 96 well plates and incubated for additional 4 h at 37 °C in a 5% CO_2 incubator. Formed formazan crystals were solubilized in DMSO after removal of the existed media and the absorbance was measured at a wavelength of 595 nm. Cell viability was calculated as, viability (%) = $100 \times A_2/A_1$; (where A_2 = absorbance of the treated cell; A_1 = absorbance of the control cells).

Cytotoxicity of photoCORMs with Photolysis. The cytotoxicity of the designed photoCORMs (**3**, **5**, and **8**) and free drug chlorambucil was using the estimated with the MTT assay. The cancerous B16F10 cells were treated with the different concentrations such as UT and 1.25, 2.5, 5, 10 μM of photoCORMs (**3**, **5**, and **8**) and chlorambucil in HEPES buffer containing 0.5% DMSO were added and incubated at 37 °C in a 5% CO_2 incubated for 6 h. Thereafter, we irradiated for 5 min using a medium pressure Hg lamp (125 W) as $\lambda \geq 365$ nm UV light source and 1 M $CuSO_4$ solution as a UV cut-off filter and further incubated for 72 h. Further, 0.4 mg/mL MTT containing DMEM was added to the 96 well plates and incubated for additional 4 h at 37 °C in a 5% CO_2 incubator. The formazan crystals formed were solubilized in DMSO after removal of the existed media and the absorbance was measured at a wavelength of 595 nm. Cell viability was calculated as, viability (%) = $100 \times A_2/A_1$; (where A_2 = absorbance of the treated cell; A_1 = absorbance of the control cells).

Apoptosis Detection Assay. HEK 293 and B16F10 cells ($\sim 1 \times 10^5$ cells/well) were plated in a 6-well plate overnight and thereafter, incubated with photoCORM **5** (5 μM containing 1 mL DMEM) with and without light irradiation. Further, the cells were trypsinized, washed (3 × 1 mL) with PBS, and centrifuged at 3000 rpm for 5 min. Then, the cell pellet was incubated with Annexin-V FITC (0.25 μg) containing binding buffer (500 μL) and 1 μg of propidium iodide in a dark place. Thereafter, the samples were analyzed using flow cytometry (BD FACS Canto II software, USA).

*Biodistribution Studies of photoCORM **5**.* B16F10 cells (2×10^5) in 100 μL HBSS was injected in the right flank of six to eight weeks old female C57BL/6 mice (n = 3). 18 days after the post tumor inoculation, when tumor volume reached ∼1500 mm^3, mice were intravenously administered with one dosage of photoCORM **5** (0.4 mg/kg BW of mice) after 24 h of post injection, Acidified isopropanol (0.5 mL) was added to the tissue and tumor samples and homogenized with a mechanical homogenizer for 60 s at 5000 beats/minute. All tissue samples were maintained at ice-cold conditions before and after the homogenization in the dark. Homogenized samples were incubated overnight in acidified isopropanol (90 percentage isopropanol, 75 mM Hydrochloric acid, 10 percentage water) at 4 °C. Then, the samples were vortexed and centrifuged (14 000 rpm) for 10 min at 4 °C; further, the supernatant (100 μL per well) was plated onto a 96-well plate in triplicate. Intravenously injected photoCORM **5** concentrations in various tissue extracts were measured by fluorescent measurement of tissues extracts at 370 nm excitation and 410 nm emission (λ_{max} of CO molecule) using a CO molecule concentration versus fluorescence standard curve. The fluorescence of tissue extracts from UT control mice was used to rectify the background fluorescence of tissue extracts.

*Tumor Growth Inhibition and Survivability Studies of the Dual photoCORM **5**.* Tumor growth inhibition and survivability are studied with six to eight weeks of old female C57BL/6J mice (weights of each group ∼22−25 g) with an aggressive B16F10 Melanoma mice model (produced by subcutaneous injections of B16F10 cells ($\sim 2 \times 10^5$) in HBSS (250 μL) into the right flanks on day 0) were arbitrarily distributed into three groups (n = 5), one group was intravenously injected with: 5 percent aqueous glucose (UT mice (n = 5), and other two groups were administered intravenously [0.4 mg/kg body weight of mice (each group n = 5)] with photoCORM **5** was given dose alternate days from the 14, 16, 18, 20, 22, and 24th days and we irradiate a 730 nm laser for 10 min for one group (n = 5) by alternate day on 15, 17, 19, 21, 23, and 25th day. Tumor volumes ($V = 1/2 \cdot ab^2$ where, a = maximum length of the tumor and b = minimum length of the tumor measured perpendicular to each other) were measured with a slide caliper for up to 24 days. On day 24, tumors of treated mice

https://doi.org/10.1021/acs.jmedchem.1c00750
J. Med. Chem. 2022, 65, 1822−1834

groups were isolated and their photographs were recorded, and remaining animals left for survivability where UT mice and dual photoCORM **5** treated mice were died around 43 days of post tumor inoculation and photoCORM **5** with irradiation treated mice survived more than the remaining group mice.

In Vivo Toxicity Study (H&E Staining). Four to six weeks old C57BL/6J mice (weights of each group ∼20 g) subcutaneously injected with B16F10 cells (2×10^5 cells) were IV administered (6 times, every alternative day from day 14th of post cells implantation) with photoCORM **5** (as described in Figure 10). During the treatment period of 24 h, there is no major variations in weights and no signs of distress in the mice were observed (data not shown). The photoCORM **5** treated mice group organs and tumors were harvested and performed the H & E staining as previously reported.[35]

Cells and Culture Media. Murine melanoma (B16F10) and HEK 293 cells (received from the National Centre for Cell Science (NCCS), Pune, India) were cultured in DMEM containing 10% FBS with the addition of pen-strep antibiotic solution. The cells were maintained in a humidified 5% CO_2 incubator at 37 °C.

Animals. 6−8 weeks old female C57BL/6J mice (weighing each 20−25 g) were selected for the study. All animal experiments were organized in accordance with the generally accepted protocols approved (**approval no. IICT/IAEC/44/2018**) by the Institutional Biosafety and Animal Ethical Committee.

■ ASSOCIATED CONTENT

Supporting Information

The Supporting Information is available free of charge at https://pubs.acs.org/doi/10.1021/acs.jmedchem.1c00750.

Molecular formula strings (CSV)

Characterization data by ^{1}H, ^{13}C NMR, and HRMS spectra of all synthesized compounds; photophysical properties; experimental details of photolysis; experimental procedures for the CO detection; HPLC trace for the photoCORMs; and quenching experiments (PDF)

■ AUTHOR INFORMATION

Corresponding Authors

Avijit Jana − *Department of Applied Biology, CSIR-Indian Institute of Chemical Technology (CSIR-IICT), Hyderabad 500007, India; Department of Organic Synthesis and Process Chemistry, CSIR-Indian Institute of Chemical Technology (CSIR-IICT), Hyderabad 500007, India; Academy of Scientific and Innovative Research (AcSIR), Ghaziabad 201002, India;* orcid.org/0000-0002-4828-2970; Email: janaavijit2@gmail.com, avijit@iict.res.in

N. D. Pradeep Singh − *Department of Chemistry, Indian Institute of Technology Kharagpur, West Bengal 721302, India;* orcid.org/0000-0001-6806-9774; Email: ndpradeep@chem.iitkgp.ac.in

Authors

Yarra Venkatesh − *Department of Chemistry, Indian Institute of Technology Kharagpur, West Bengal 721302, India;* orcid.org/0000-0002-4478-1553

Venugopal Vangala − *Department of Applied Biology, CSIR-Indian Institute of Chemical Technology (CSIR-IICT), Hyderabad 500007, India; Academy of Scientific and Innovative Research (AcSIR), Ghaziabad 201002, India;* orcid.org/0000-0001-9701-2136

Rakesh Mengji − *Department of Applied Biology, CSIR-Indian Institute of Chemical Technology (CSIR-IICT), Hyderabad 500007, India; Academy of Scientific and Innovative Research (AcSIR), Ghaziabad 201002, India*

Amrita Chaudhuri − *Department of Chemistry, Indian Institute of Technology Kharagpur, West Bengal 721302, India*

Sayantan Bhattacharya − *Department of Physics, Indian Institute of Technology Kharagpur, West Bengal 721302, India*

Prasanta Kumar Datta − *Department of Physics, Indian Institute of Technology Kharagpur, West Bengal 721302, India;* orcid.org/0000-0001-9476-7656

Rajkumar Banerjee − *Department of Applied Biology, CSIR-Indian Institute of Chemical Technology (CSIR-IICT), Hyderabad 500007, India; Academy of Scientific and Innovative Research (AcSIR), Ghaziabad 201002, India;* orcid.org/0000-0003-2336-6294

Complete contact information is available at: https://pubs.acs.org/10.1021/acs.jmedchem.1c00750

Author Contributions

#Y.V. and V.V. contributed equally to this work. The manuscript was written through the contributions of all authors. All authors have approved the final version of the manuscript.

Notes

The authors declare no competing financial interest.

■ ACKNOWLEDGMENTS

The authors thank the DST SERB (grant nos. EMR/2016/005885 & DIA/2018/000019) for financial support. Y.V. is thankful to the Indian Institute of Technology Kharagpur for the fellowship. A.J. and R.M. thank DST for the INSPIRE Faculty Grant (IFA15, CH171, GAP0546). VVG thanks UGC for the fellowship. R.M. thanks CSIR for the fellowship. The authors are thankful to Dr. Arabinda Chaudhuri for his valuable suggestions. The CSIR-IICT Communication number for this manuscript is IICT/Pubs./2020/132.

■ ABBREVIATIONS

CLSM, confocal laser scanning microscopy; MTT, 3-(4,5-dimethylthiazol-2-yl)-2,5-diphenyltetrazolium bromide; CORMs, carbon monoxide releasing molecules; DMEM, Dulbecco's modified eagle's medium; FBS, fetal bovine serum; HBSS, Hank's buffer salt solution; HPLC, high-performance liquid chromatography; NMR, nuclear magnetic resonance; HRMS, high-resolution mass spectrometry; TPA, two-photon absorption; DPA, 9,10-diphenylanthracene; H&E, haematoxylin and eosin; PNPCl4-nitrophenyl chloroformate, 4-nitrophenyl chloroformateDBU,1,8-diazabicyclo [5.4.0] undec-7-ene; CORM-3, Tricarbonylchloro(glycinato)-ruthenium (II); MbCO, carbonmonoxy-myoglobin; MbFe(II), deoxy-myoglobin; δ_a, TPA cross-section; δ_u, two-photon uncaging cross-section; OA, open aperture; Cys, cysteine; Hcys, homocysteine; GSH, glutathione; cbl, chlorambucil; GM, Goeppert-Mayer; NIR, near infrared

■ REFERENCES

(1) Motterlini, R.; Otterbein, L. E. The therapeutic potential of carbon monoxide. *Nat. Rev. Drug Discovery* **2010**, *9*, 728−743.

(2) Ryter, S. W.; Alam, J.; Choi, A. M. K. Heme oxygenase-1/carbon monoxide: from basic science to therapeutic applications. *Physiol. Rev.* **2006**, *86*, 583−650.

(3) Ji, X.; Wang, B. Strategies toward organic carbon monoxide prodrugs. *Acc. Chem. Res.* **2018**, *51*, 1377−1385.

(4) Wegiel, B.; Gallo, D.; Csizmadia, E.; Harris, C.; Belcher, J.; Vercellotti, G. M.; Penacho, N.; Seth, P.; Sukhatme, V.; Ahmed, A.; Pandolfi, P. P.; Helczynski, L.; Bjartell, A.; Persson, J. L.; Otterbein, L. E. Carbon monoxide expedites metabolic exhaustion to inhibit tumor growth. *Cancer Res.* **2013**, *73*, 7009−7021.
(5) Zheng, Y.; Ji, X.; Yu, B.; Ji, K.; Gallo, D.; Csizmadia, E.; Zhu, M.; Choudhury, M. R.; De La Cruz, L. K. C.; Chittavong, V.; Pan, Z.; Yuan, Z.; Otterbein, L. E.; Wang, B. Enrichment-triggered prodrug activation demonstrated through mitochondria-targeted delivery of doxorubicin and carbon monoxide. *Nat. Chem.* **2018**, *10*, 787−794.
(6) Li, Y.; Dang, J.; Liang, Q.; Yin, L. Thermal-responsive carbon monoxide (CO) delivery expedites metabolic exhaustion of cancer cells toward reversal of chemotherapy resistance. *ACS Cent. Sci.* **2019**, *5*, 1044−1058.
(7) Vítek, L.; Gbelcová, H.; Muchová, L.; Váňová, K.; Zelenka, J.; Koníčková, R.; Šuk, J.; Zadinova, M.; Knejzlík, Z.; Ahmad, S.; Fujisawa, T.; Ahmed, A.; Ruml, T. Antiproliferative effects of carbon monoxide on pancreatic cancer. *Dig. Liver Dis.* **2014**, *46*, 369−375.
(8) Romanski, S.; Kraus, B.; Schatzschneider, U.; Neudörfl, J.-M.; Amslinger, S.; Schmalz, H.-G. Acyloxybutadiene iron tricarbonyl complexes as enzyme-triggered CO-releasing molecules (ET-CORMs). *Angew. Chem., Int. Ed.* **2011**, *50*, 2392−2396.
(9) Kunz, P. C.; Meyer, H.; Barthel, J.; Sollazzo, S.; Schmidt, A. M.; Janiak, C. Metal carbonyls supported on iron oxide nanoparticles to trigger the CO-gasotransmitter release by magnetic heating. *Chem. Commun.* **2013**, *49*, 4896−4898.
(10) Ji, X.; Pan, Z.; Yu, B.; De La Cruz, L. K.; Zheng, Y.; Ke, B.; Wang, B. Click and release: bioorthogonal approaches to "on-demand" activation of prodrugs. *Chem. Soc. Rev.* **2019**, *48*, 1077−1094.
(11) Chakraborty, I.; Carrington, S. J.; Mascharak, P. K. Design strategies to improve the sensitivity of photoactive metal carbonyl complexes (photoCORMs) to visible light and their potential as CO-donors to biological targets. *Acc. Chem. Res.* **2014**, *47*, 2603−2611.
(12) Mann, B. E. CO-releasing molecules: a personal view. *organometallics* **2012**, *31*, 5728−5735.
(13) Poloukhtine, A. A.; Mbua, N. E.; Wolfert, M. A.; Boons, G.-J.; Popik, V. V. Selective labeling of living cells by a photo-triggered click reaction. *J. Am. Chem. Soc.* **2009**, *131*, 15769−15776.
(14) Kuzmanich, G.; Garcia-Garibay, M. A. Ring strain release as a strategy to enable the singlet state photodecarbonylation of crystalline 1,4-cyclobutanediones. *J. Phys. Org. Chem.* **2011**, *24*, 883−888.
(15) Torres, M.; Clement, A.; Strausz, O. P. Photolysis of vinylene thioxocarbonates: a new source of ketocarbenes. *J. Org. Chem.* **1980**, *45*, 2271−2273.
(16) Chapman, O. L.; Wojtkowski, P. W.; Adam, W.; Rodriguez, O.; Rucktaeschel, R. Photochemical transformations. XLIV. Cyclic peroxides. Synthesis and chemistry of .alpha.-lactones. *J. Am. Chem. Soc.* **1972**, *94*, 1365−1367.
(17) Peng, P.; Wang, C.; Shi, Z.; Johns, V. K.; Ma, L.; Oyer, J.; Copik, A.; Igarashi, R.; Liao, Y. Visible-light activatable organic CO-releasing molecules (PhotoCORMs) that simultaneously generate fluorophores. *Org. Biomol. Chem.* **2013**, *11*, 6671.
(18) Antony, L. A. P.; Slanina, T.; Šebej, P.; Šolomek, T.; Klán, P. Fluorescein analogue xanthene-9-carboxylic acid: a transition-metal-free CO releasing molecule activated by green light. *Org. Lett.* **2013**, *15*, 4552−4555.
(19) Lazarus, L. S.; Esquer, H. J.; Benningho, A. D.; Berreau, L. M. Sense and release: a thiol-responsive flavonol-based photonically driven carbon monoxide-releasing molecule that operates via a multiple-input AND logic gate. *J. Am. Chem. Soc.* **2017**, *139*, 9435−9438.
(20) Soboleva, T.; Benninghoff, A. D.; Berreau, L. M. An H 2 S-Sensing/CO-Releasing Flavonol That Operates via Logic Gates. *ChemPlusChem* **2017**, *82*, 1408−1412.
(21) Feng, W.; Feng, S.; Feng, G. CO release with ratiometric fluorescence changes: a promising visible-light-triggered metal-free CO-releasing molecule. *Chem. Commun.* **2019**, *55*, 8987−8990.
(22) Popova, M.; Lazarus, L. S.; Ayad, S.; Benninghoff, A. D.; Berreau, L. M. Visible-light-activated quinolone carbon-monoxide-releasing molecule: prodrug and albumin-assisted delivery enables anticancer and potent anti-inflammatory effects. *J. Am. Chem. Soc.* **2018**, *140*, 9721−9729.
(23) Momotake, A.; Lindegger, N.; Niggli, E.; Barsotti, R. J.; Ellis-Davies, G. C. R. The nitrodibenzofuran chromophore: a new caging group for ultra-efficient photolysis in living cells. *Nat. Methods* **2006**, *3*, 35−40.
(24) Klán, P.; Šolomek, T.; Bochet, C. G.; Blanc, A.; Givens, R.; Rubina, M.; Popik, V.; Kostikov, A.; Wirz, J. Photoremovable protecting groups in chemistry and biology: reaction mechanisms and efficacy. *Chem. Rev.* **2013**, *113*, 119−191.
(25) Abe, M.; Chitose, Y.; Jakkampudi, S.; Thuy, P.; Lin, Q.; Van, B.; Yamada, A.; Oyama, R.; Sasaki, M.; Katan, C. Design and synthesis of two-photon responsive chromophores for near-infrared light-induced uncaging reactions. *Synthesis* **2017**, *49*, 3337−3346.
(26) Palao, E.; Slanina, T.; Muchová, L.; Šolomek, T.; Vítek, L.; Klán, P. Transition-metal-free CO-releasing BODIPY derivatives activatable by visible to NIR light as promising bioactive molecules. *J. Am. Chem. Soc.* **2016**, *138*, 126−133.
(27) Li, Y.; Shu, Y.; Liang, M.; Xie, X.; Jiao, X.; Wang, X.; Tang, B. A Two-Photon H2 O2 -Activated CO Photoreleaser. *Angew. Chem., Int. Ed.* **2018**, *57*, 12415−12419.
(28) Venkatesh, Y.; Rajesh, Y.; Karthik, S.; Chetan, A. C.; Mandal, M.; Jana, A.; Singh, N. D. P. Photocaging of single and dual (similar or different) carboxylic and amino acids by acetyl carbazole and its application as dual drug delivery in cancer therapy. *J. Org. Chem.* **2016**, *81*, 11168−11175.
(29) Venkatesh, Y.; Nandi, S.; Shee, M.; Saha, B.; Anoop, A.; Pradeep Singh, N. D. Bis-Acetyl Carbazole: A Photoremovable Protecting Group for Sequential Release of Two Different Functional Groups and Its Application in Therapeutic Release. *Eur. J. Org. Chem.* **2017**, *2017*, 6121−6130.
(30) Wen, P.; Gao, Z.; Zhang, R.; Li, A.; Zhang, F.; Li, J.; Xie, J.; Wu, Y.; Wu, M.; Guo, K. A-π-D-π-A carbazole derivatives with remarkable solvatochromism and mechanoresponsive luminescence turn-on. *J. Mater. Chem. C* **2017**, *5*, 6136−6143.
(31) Romanet, R.; Bahut, F.; Nikolantonaki, M.; Gougeon, R. D. Molecular Characterization of White Wines Antioxidant Metabolome by Ultra High Performance Liquid Chromatography High-Resolution Mass Spectrometry. *Antioxidants* **2020**, *9*, 115.
(32) Samanta, S.; Mondal, S.; Hajra, A. A convergent synthesis of vinyloxyimidazopyridine via Cu(I)-catalyzed three-component coupling. *Org. Biomol. Chem.* **2018**, *16*, 1088−1092.
(33) Venkatesh, Y.; Srivastava, H. K.; Bhattacharya, S.; Mehra, M.; Datta, P. K.; Bandyopadhyay, S.; Singh, N. D. P. One- and two-photon uncaging: carbazole fused *o*-hydroxycinnamate platform for dual release of alcohols (same or different) with real-time monitoring. *Org. Lett.* **2018**, *20*, 2241−2244.
(34) Feng, S.; Liu, D.; Feng, W.; Feng, G. Allyl fluorescein ethers as promising fluorescent probes for carbon monoxide imaging in living cells. *Anal. Chem.* **2017**, *89*, 3754−3760.
(35) Mengji, R.; Acharya, C.; Vangala, V.; Jana, A. A lysosome-specific near-infrared fluorescent probe for in vitro cancer cell detection and non-invasive in vivo imaging. *Chem. Commun.* **2019**, *55*, 14182−14185.

https://doi.org/10.1021/acs.jmedchem.1c00750
J. Med. Chem. 2022, 65, 1822−1834